Explanation of commonly observed shunt currents in c-Si solar cells by means of recombination statistics beyond the Shockley-Read-Hall approximation

Silke Steingrube,[1,a)] Otwin Breitenstein,[2] Klaus Ramspeck,[3,b)] Stefan Glunz,[4] Andreas Schenk,[5] and Pietro P. Altermatt[5]
[1]*Department Solar Energy, Institute Solid-State Physics, Leibniz University of Hannover, Appelstr. 2, 30167 Hannover, Germany*
[2]*Max-Planck-Institute of Microstructure Physics, Weinberg 2, 06120 Halle, Germany*
[3]*Institute for Solar Energy Research Hamelin (ISFH), Am Ohrberg 1, 31860 Emmerthal, Germany*
[4]*Fraunhofer Institute for Solar Energy Systems (ISE), Heidenhofstr. 2, 79110 Freiburg, Germany*
[5]*Integrated Systems Laboratory, ETH Zurich, Gloriastr. 35, 8092 Zurich, Switzerland*

(Received 11 May 2011; accepted 31 May 2011; published online 15 July 2011)

The current-voltage (I–V) characteristics of industrially fabricated, crystalline silicon solar cells are often influenced by non-linear shunts that originate from localized, highly disturbed regions and cause ideality factors $n > 2$. We show that recombination within such locations needs model descriptions that go beyond the Shockley-Read-Hall (SRH) approximation, because the density of defects is so high that recombination does not occur via isolated, but coupled defect states. We use a variant of coupled defect level (CDL) recombination, the donor-acceptor-pair (DAP) recombination, but via deep levels (as opposed to shallow levels). With this model, we quantitatively reproduce the I–V curves of solar cells that we subjected to various degrees of cleaving, laser scribing or diamond scratching to form shunt locations in a controlled manner. The suggested model explains the transition from ideality factors $n < 2$ to $n > 2$ when going from low to high defect densities. We also explain the non-saturating reverse I–V characteristics. We show that an additional source of currents with $n > 2$ is SRH recombination in an inversion layer that extends from the front p-n junction to the rear contact along the cell's edge or along a micro-crack.
 [doi:10.1063/1.3607310]

I. INTRODUCTION

The well-known Shockley-Read-Hall (SRH) recombination model[1,2] quantifies the recombination rate in semiconductor materials via a single defect level. When this model is applied to recombination in the space charge region of p-n junction diodes, it influences the ideality factor n of the current-voltage (I-V) curve, described by the Shockley equation:[3]

$$j(V) = j_0 \left[\exp\left(\frac{V}{nV_{th}} \right) - 1 \right] \quad (1)$$

Here, j_0 is the saturation current-density, j the current density I/A, $V_{th} = kT/q$ the thermal voltage, where k is Boltzmann's constant, q the elementary charge, and T is the absolute temperature. It was demonstrated in various attempts[4–10] that n can reach but not exceed 2. For an overview on such attempts see Ref. 11.

In contrast to these theoretical findings, it has been well-known for more than 40 years[12] that the forward-characteristics may show an n value larger than 2, up to values of about 5, over an extended voltage range. This is observed in most industrially fabricated Si solar cells and frequently also in cell designs under development. Moreover, the reverse characteristics are in these cases Ohmic or slightly super-linear, which cannot be described within the SRH model either: it predicts saturation behavior.

Previous attempts to explain large ideality factors were made with various models, including trap-assisted tunneling,[13] field-enhanced recombination,[14] saturation effects within the SRH-model for donor-like levels,[15] resistance-limited action of SRH-type edge recombination currents,[16–18] and bias-dependent band bending that extends the recombination region to the p-type surface.[19] In some of these models (Refs. 13–15), it was assumed that the point defects are more or less homogeneously distributed in the whole depletion region. However, as it was suggested already in 1962,[12] the currents having $n > 2$ do not originate from a homogeneous distribution of defects, but from local sites with a very high defect density. This was experimentally confirmed by means of lock-in thermography.[20–23] For example, it was found that an increased recombination current can be observed in the whole edge region, but the edge current-density distinctly peaks at a few sites at the edge, which are called local edge shunts.[21,22] Ideality-factor mapping performed by lock-in thermography showed that n is generally larger than 2 only in these local edge shunts, whereas there is $n \lesssim 2$ in the other edge regions as expected from SRH theory.[21]

[a)]Electronic mail: steingrube@solar.uni-hannover.de
[b)]Now with: SCHOTT Solar AG, Division Technology/Research and Development, Carl-Zeiss-Str. 4, 63755 Alzenau, Germany

In this paper, we verify the local nature of shunts by disturbing the p-n junction depletion region in the interior part of cells in a controlled and reproducible manner by cleaving, laser scribing, or diamond scratching of the front surface above the shallow diffused emitter. We propose that the source of currents with $n > 2$ are defects that are coupled together and therefore cannot be described by the SRH theory. Defects with energy levels deep in the forbidden bandgap have a very localized wave function and therefore act in general as isolated entities. A remarkable coupling between the defects occurs if their density becomes so high that their wave functions overlap. This is indeed the case in local shunt areas: oxidized surfaces may already show a density of defect states of about 10^{12} cm^{-2}, corresponding to a mean distance between the defects of 10 nm. A highly disturbed region may easily have a hundredfold higher defect density, corresponding to a mean distance below 1 nm. This makes interaction among deep defects very likely. We reproduce our measured currents with a model of donor-acceptor-pair (DAP) recombination, but via deep levels (as opposed to the usually treated shallow levels [24,25]).

To avoid ambiguities, we define a shunt in a diode as any path where carriers flow as an alternative to being fully injected across the p-n junction.[16] This implies that not all currents having $n > 2$ are shunts. For example, the recombination rate at oxidized Si back surfaces shows a saturation behavior and can cause $n > 2$ if this rate is dominating the cell's total recombination rate.[26,27] Such current-paths do not provide an alternative to being injected across the p-n junction since the recombination occurs after the carriers are injected. In contrast, if such a surface is situated in the p-n junction depletion region, recombination may provide a short-cut for carriers through the p-n junction, so they do not need to be thermally excited above the entire potential barrier across the p-n junction.[28] In this work, we deal solely with recombination currents that are shunts.

II. EXPERIMENTS

In our experiments, we have selected seven identical, 1 cm^2 sized, laboratory PERL cells which show no significant shunt currents. The I–V characteristics of all these cells, obtained at room temperature in the dark, corresponded initially to the "virgin" curve shown in Fig. 1. In order to induce shunt currents, three of these cells were disturbed in three different ways:

(1) cleavage in the (100) direction (after scratching the backside), so that the cleaved surface crosses the p-n junction depletion region over a length of 1 cm;
(2) laser-cutting through the diffused emitter into the p-n junction depletion region (1 mm along the front surface between two metal fingers);
(3) diamond scratching through the diffused emitter into the p-n junction depletion region (3 mm long at the front surface between two metal fingers).

These treatments affect the I–V curves both in forward and reverse direction, as shown in Fig. 1(a) and 1(c). We do not deduce the ideality factor n with the commonly applied formula that is derived from Eq. (1) by neglecting the offset $-j_0$:

$$n(V_i) = \frac{V_i - V_{i-1}}{V_{th} \ln[j(V_i)/j(V_{i-1})]}. \tag{2}$$

The subscripts V_i and V_{i-1} denote neighboring voltage points of the measured I-V curve and $j(Vi)$, $j(V_{i-1})$ are the corresponding current densities. As this equation is only valid at $V > 3V_{th}$, we use a formulation[29] that accounts for the offset $-j_0$:

$$n(V_i) = \frac{V_i - V_{i-1}}{V_{th} \ln\left[\frac{j(V_i)\left(1-e^{-V_{i-1}/V_{th}}\right)}{j(V_{i-1})\left(1-e^{-V_i/V_{th}}\right)}\right]}, \tag{3}$$

and hence is also valid near 0 V and at reverse bias. As expected, the virgin cell shows an n considerably smaller than 2 over the whole measured bias range, because there is no significant shunt current contribution (the small peak near 0.41 V is due to recombination saturation at the rear oxidized surface,[30] the increase toward very low voltages is due to SRH recombination in the p-n junction depletion region, which is a unavoidable recombination current). Its lock-in thermography image in Fig. 2 shows a homogeneous thermal signal across its whole area. Its reverse current is very low (in the nA range) up to many volts.

After disturbing, the thermography images confirm that the additionally created currents are limited to the disturbed regions. In Fig. 1, there is a clear correlation between the magnitude of the recombination current and the ideality factor: the higher the current, the larger the ideality factor. Cleaving produces the lowest recombination current per length unit and also the lowest n, while diamond scratching produces the highest current and the largest n. From SEM micro-graphs (not shown here) it is apparent that cleaving disturbs the p-n junction depletion region the least, while diamond scratching the most. With the assumption that cleaving introduces the smallest density of defects, and scratching the largest, we conclude that the higher the defect density, the higher is n. In addition, the increase of the reverse I-V curve is stronger the higher n at forward bias.

In a separate experiment, we used a Vickers indenter to scratch each of three cells at room temperature along a line of 1 mm with the predefined forces of 0.06 N, 0.09 N, or 0.26 N. The largest force caused a 1 μm deep scratch through the p-n junction depletion region.[31] In this way, we are able to increase the damage in a controlled manner. This experiment and its interpretation will be discussed in Sec. III C.

III. THEORETICAL DESCRIPTION OF SHUNT CURRENTS

A correlation between n and the magnitude of a local recombination current similar to that described in II is described by resistance-limited recombination,[16,17] where a larger current is more resistance-limited. While we acknowledge that this model describes some relevant situations, we observe that it does not explain the most commonly observed experimental findings. For example, the resistance-limitation

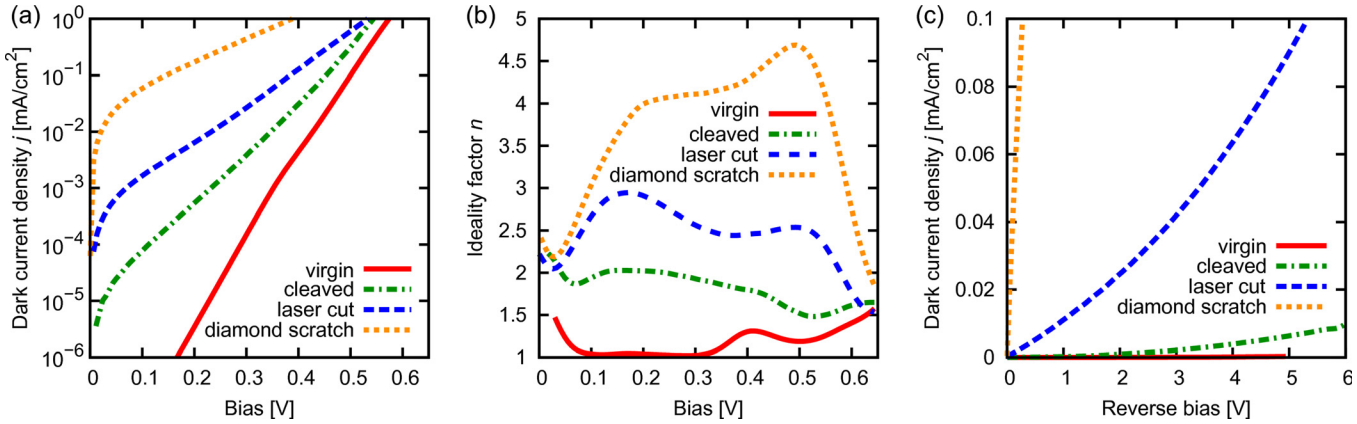

FIG. 1. (Color online) Measured dark I–V characteristics of identical 1 cm^2 sized PERL cells except that their p-n junction depletion region was damaged in various ways to generate recombination shunts in a controlled and reproducible manner. (a) The forward I–V curves in the dark, (b) the ideality factor obtained from (a) using Eq. (3), and (c) the reverse I–V curves.

appears only at a forward bias above 0.2 V, where the current is sufficiently high for this effect to become dominating, while typical measured I–V curves show $n > 2$ already below 0.1 V, as displayed in Fig. 1(a). In addition, the induced shunt locations have a very simple geometry: the scratch lies in parallel to the two neighboring metal fingers and shows a homogeneous recombination activity across its entire length in Fig. 2. Hence, its series resistance can be described by a single resistor rather than by a distribution of various resistors, which would be necessary in the resistance-limited model for explaining $n > 2$ over an extended bias range.

As the features in Fig. 1 cannot be described by series resistance effects, we need to resort to recombination that increases sub-exponentially with applied bias V, i.e., leads to a "saturation behavior" in the dark current. In the SRH formalism, the recombination rate R_{SRH} is proportional to the excess carrier density Δn at low-injection conditions, and there is no saturation behavior possible except in space charge regions where n or p saturate with increasing V (e.g., at interfaces to charged dielectrics). However, if two defect states are coupled, there exist additional capture and emission processes as shown in Fig. 3. The recombination rate may become limited by the coupling rate from one to the other defect, at sufficiently high excess carrier densities Δn, which results in the desired saturation behavior. With increasing Δn, the recombination rate R may become limited by one of the three transitions highlighted in Figs. 3(a) and 3(b), respectively. Consider as an example the transitions A→B→C in Fig. 3(a) and let the DAP be in a dipole state (i.e., the donor and the acceptor are both ionized). Given that c_n^D and c_p^A are large (A,C), recombination may become limited by the inter-defect coefficient c_{DA} for $E_A < E_D$, and by e_{DA} for $E_A > E_D$ (B), respectively. This leads to a saturation behavior in the recombination currents at sufficiently high Δn, e.g. sufficiently high forward bias voltages. We model the dark current using the Coupled Defect Level (CDL) recombination model of Ref. 14, given therein by the equations (19), (23)–(25). Apart from the coupling, these statistics satisfy the assumptions of the SRH theory, e.g., the energy levels are constant and independent of each other, the capture coefficients are also constant and independent of the occupancy of the coupled states, etc. In reality, the energy of one level will depend on the occupancy state of the other level, where the Coulomb interaction energy may be in the order of 100 meV. However, as we will show in Sec. III B, DAPs with energy levels within a broad range allow for the occurrence of $n > 2$. Hence, the simplification of constant energy levels is a valid approximation.

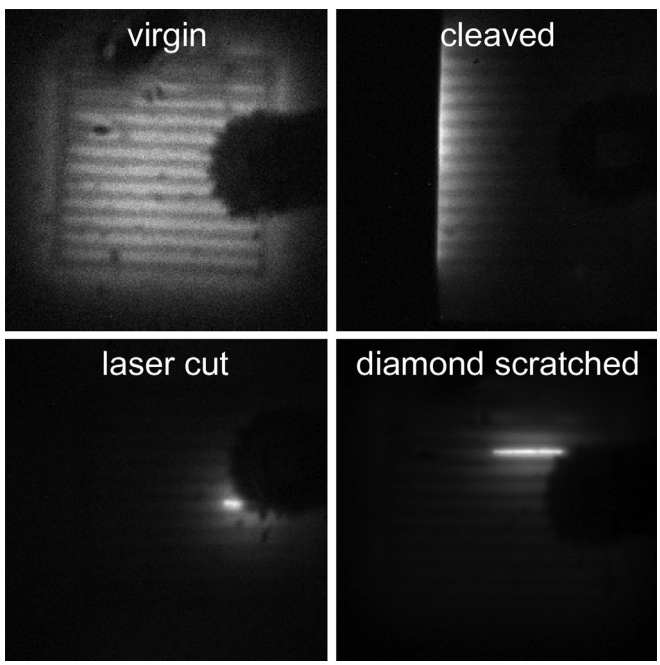

FIG. 2. Lock-in thermography images of the cells whose I-V curves are shown in Fig. 1. Bright areas are caused by heat due to excessive recombination. Note that the brightness scaling is not the same in the virgin cell (with identical scaling the cell would appear completely black).

The question now is, which properties the capture and emission processes of the two coupled defects need to possess to cause the observed shunt currents. To answer this, we can restrict ourselves to the type of defects that cause the highest recombination rates. In the SRH formalism, the probability that a defect state captures an electron or hole is given by the capture cross sections (CCS) σ_n and σ_p. These σ values are influenced by two main factors: the charge residing

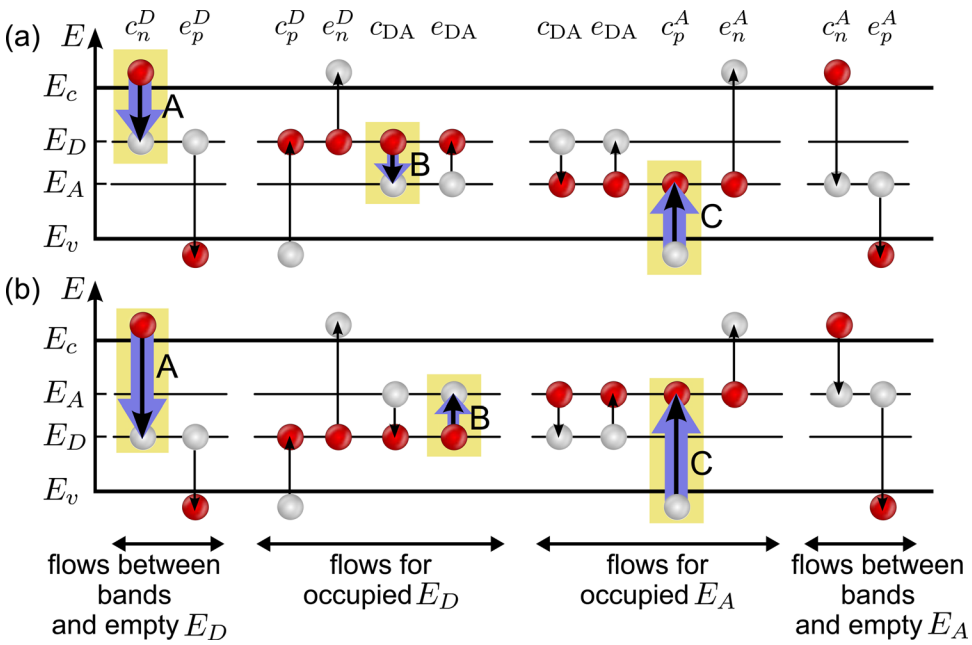

FIG. 3. (Color online) Band diagram with all charge carrier transitions considered for the case that (a) the donor is lying above the acceptor and that (b) the donor is lying below the acceptor. White balls indicate empty states and red balls indicate states that are occupied by an electron. The capture and emission coefficients are labeled above the sketch. The transitions dominating for low forward biases are marked and the purple arrows illustrate the occurrence of saturation behavior.

in the defect state, and the overlap of its wave function with the wave function of the incoming carrier. A literature review shows[32] that it is mainly the charge that controls σ in deep-lying defect states. Concretely, a positively charged defect level is more likely to attract electrons than holes, i.e., $\sigma_n > \sigma_p$.[33] As the capture probability of electrons and holes is given by the CCS, we propose that the recombination rate is dominated by sites where an acceptor-like defect (with $\sigma_n \ll \sigma_p$) is coupled to a donor-like defect (with $\sigma_n \gg \sigma_p$). Consider, as an example, the transitions highlighted in Fig. 3 for the case that the acceptor lies below the donor [Fig. 3(a)] or above the donor [Fig. 3(b)]. Due to the asymmetric CCS, the donor-like state captures electrons likely (A), transfers this electron to the acceptor-like defect (B), which is then likely to capture a hole (C). The recombination via this type of coupled defect is described in the literature as DAP recombination.[24,25] However, these references consider shallow defects, which have a well extended wave function. We will show below that the experimentally observed shunt currents cannot be explained with shallow defects. Instead, we require *deep-lying* donor-like and acceptor-like defects, which have constricted wave functions and, accordingly, need to exist both in very high densities to couple to each other. Therefore, we need to extend the DAP recombination model with dependencies on defect density, as is done in the following.

A. Dependencies on the defect density

With an increasing density of defects, the experiments in Section II show a transition from SRH-like recombination via isolated defects ($n \leq 2$) to recombination with $n > 2$. To include this effect in the simulations, we introduce physically motivated dependencies between the recombination parameters and the defect density. We assume that both the CCS and the coupling parameter r_{DA} depend on the distance between donor and acceptor r.[25] We use the same notation as Ref. 14, but replace the subscript "1" of the first defect with "D" (donor-like) and the subscript "2" of the second defect with "A" (acceptorlike).

The effective charge state of coupled pairs sensed by free charge carriers is a function of r. For r much larger than the distance between the charge carrier and one of the defects ($r \gg r_c$), the CCS will be that of the isolated donor and acceptor ($\sigma_{n,p}^{0,D}, \sigma_{n,p}^{0,A}$, respectively).[25] For small separations ($r \ll r_c$), however, the defect pair appears "neutral" leading to a much smaller capture cross section. Note that if a dipole is formed as in case of Fig. 3(a) (an electron tunnels from the donor to the acceptor), "neutral" refers to the fact that the electron senses only the monopole. We assume here that the free charge carriers are captured by the pair of defects. This is valid as long as the DAP concentrations are much larger than the concentrations of the free charge carriers. Following the empirical relation proposed by Ref. 25, we assume the CCS *for pairs* to be proportional to the square of r[25]:

$$\sigma_{n,p}(r) = \sigma_{n,p}^{0}\left(\frac{r}{r_0}\right)^2 := Ar^2. \tag{4}$$

The case $r \to \infty$ is no problem, since Eq. (4) only refers to the CCS for electrons and holes of the donor and acceptor in a coupled DAP, where large distances between the defects in a pair are unlikely. (For large distances, the exponent of (r/r_0) should be zero instead of two.)

The σ-values can then be expressed as carrier lifetime parameters

$$\tau_{n,p} = \left(N_{\mathrm{DAP}}\sigma_{n,p}v_{th,n,p}\right)^{-1}, \tag{5}$$

where $N_{DAP} = N_t/2$ is the DAP density, N_t is the sum of the defect density of the donor and acceptor-like defects, and v_{th} is the thermal velocity.

Further, we assume that once a free carrier is captured by the pair, it depends on the charge type of the free carrier whether it is captured by the donor or acceptor. If for example an electron is captured by the pair, one may say that it is captured rather by the donor, because the coupling of the free electron to the wave function of the pair has to be taken into account. The probability of finding the electron of an ionized donor acceptor pair is highest close to the acceptor. Thus, the part of the wave function located at the donor couples strongest to the additionally captured electron. We model this by assuming an asymmetric ratio of the CCS σ_n/σ_p with values ranging from 10^3 to 10^{12} for donors *in a pair*. Inverse ratios are used for the acceptors. Note that these high ratios cannot be measured, because for *isolated* defect levels, the asymmetry of this ratio is $10^{-4} < \sigma_n/\sigma_p < 10^4$. We also assume that the coupling coefficient r_{DA} in units of $cm^{-3}s^{-1}$ is $r_{DA} = c_{DA}N_D N_A$,[14] where the down coefficient (in units of cm^3s^{-1}), c_{DA}, is proportional to the overlap integral of the wave functions. Assuming further H-like radial-symmetric wave functions for the defects, the first radial wave-function reads:

$$R_{10}(\varrho) = 2\left(\frac{Z}{a_0}\right)^{3/2} \exp\left(-\frac{Z\varrho}{a_0}\right), \tag{6}$$

where a_0 is the Bohr radius of the donor or acceptor and ϱ is the spherical coordinate of the H atom. Assuming $Z = 1$ for ionized defects, the overlap integral of the wave functions results in:[34]

$$L(r) = \left[1 + \frac{r}{a_0} + \frac{1}{3}\left(\frac{r}{a_0}\right)^2\right] \exp\left(-\frac{r}{a_0}\right). \tag{7}$$

Here, we assumed an equal extension for acceptor- and donor-like defects (i.e., equal Bohr radii). This is not satisfied in general, but it is a valid simplification here, because a_0 is unknown and therefore a fitting parameter. Finally, we obtain the following definition of the capture probability c_{DA}:

$$c_{DA}(r) = c_{DA}^0 L(r) \tag{8}$$

Figure 4 shows the dependence of the coupling constant r_{DA} and the capture cross section, expressed as carrier lifetime parameters Eq. (5), on the distance between the two coupled defects d_t.

We use the numerical device simulator Sentaurus-Device[35] to simulate the I-V curves of the solar cell used in the experiments in Sec. II. See Fig. 5(a) for the simulation domain and Refs. 36 and 37 for the model parameters. The damaged region covers an adjustable fraction of the entire simulation domain. Figure 6(a) shows the simulation results with an increasing density of defect states N_t. The CCS and the coupling constant r_{DA} vary with N_t according to Eqs. (4)–(8). In this example, the energy levels are $E_D = 100$ meV and $E_A = 0$ meV, where we define $E = 0$ eV as midgap. The corresponding ideality factors shown in Fig. 6(b) are obtained from Fig. 6(a) using Eq. (3). The following features become apparent. For the lowest defect densities, $N_t = 10^{18}$ cm^{-3}, the distance between the defects is as large as at oxidized surfaces

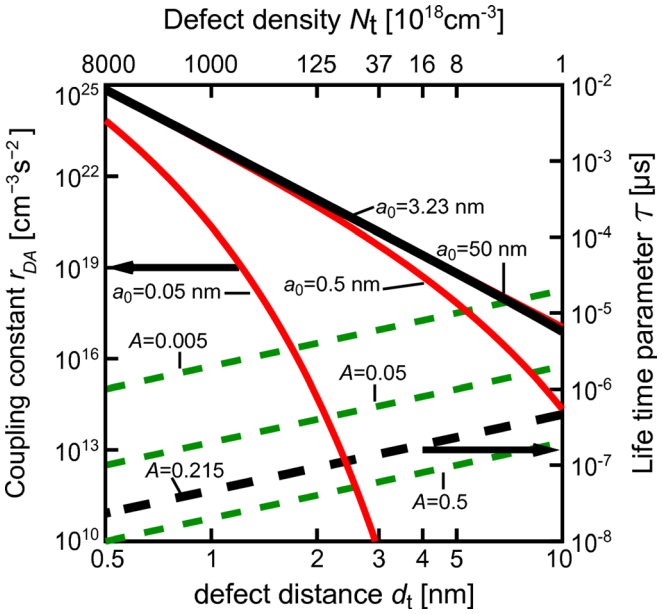

FIG. 4. (Color online) Dependence of the coupling constant r_{DA} (red solid lines) and the carrier lifetime parameters [Eq. (5)] (dashed green lines) on the distance between the coupled defects d_t, for various values of the the Bohr radius of the defect, a_0 in Eq. (6), and the proportionality constant of the capture cross section, A in Eq. (4). c_{DA}^0 is fixed to 1.1×10^{-19} cm^3/s. The parameters chosen for the simulations ($A = 0.215$, $a_0 = 3.23$ nm) are indicated by bold black lines.

(10 nm), and the overlap of the wave function is too small to lead to noticeable coupling. In this limit the CDL model results in vanishing recombination, hence the ideality factor becomes $n = 1$. Note that no additional single-level recombination processes have been taken into account. With higher N_t, the CDL recombination starts dominating the other recombination mechanisms in the cell (SRH and Auger) and this

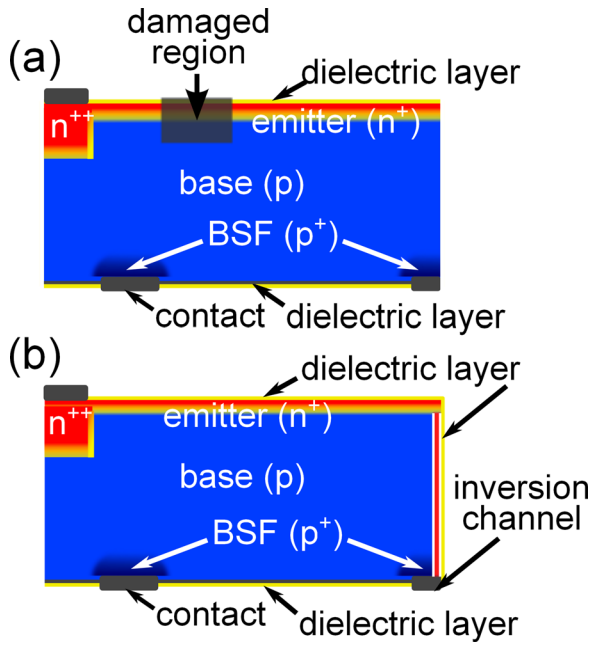

FIG. 5. (Color online) Simulation domain of the PERL cells used in Sec. II with either (a) a partly damaged p-n junction depletion region, or (b) a dielectric layer along the cell's edge, causing an inversion channel between the emitter and the p-contact at the rear. Not drawn to scale.

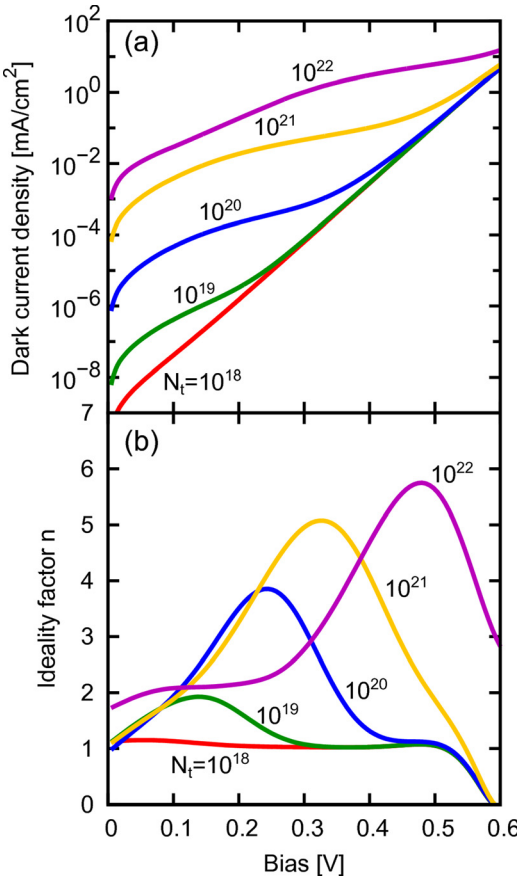

FIG. 6. (Color online) Dark current density and ideality factor n in dependence of the bias voltage for various defect densities N_t. The energy levels of the defects are $E_D = 100$ meV, $E_A = 0$ meV. The parameters for the density dependence of the recombination parameters according to Eqs. (4)–(8) are set to $c^0_{DA} = 1.1 \times 10^{-19}$ cm^3/s, $A = 0.215$, $a_0 = 3.23$ nm (Fig. 4). An asymmetry of the free-to-bound CCS of $\sigma^D_n/\sigma^D_p = \sigma^A_p/\sigma^A_n = 10^{12}$ is assumed, and $E = 0$ at midgap.

leads to the desired saturation behavior. Note that $n > 2$ appears already at biases below 0.1 V where the resistance-limited edge recombination does not show any effect.[16,17] Both, the recombination current and the maximal ideality factor increase with increasing N_t, mostly caused by the increased coupling coefficient r_{DA}. $N_t = 10^{22}$ cm^{-3} is chosen as an upper limit in order not to exceed the density of silicon atoms ($N_{Si} \approx 5 \times 10^{22}$ cm^{-3}).

B. Dependencies on the energy levels

For a fixed defect density of $N_t = 10^{21}$ cm^{-3}, the energy levels of the defects are varied from –200 meV to +300 meV in Fig. 7. A few features become apparent. The currents are largest near $E_A = E_D + 100$ meV. When E_A is moved below E_D, the current at given voltages decreases slowly with the energy separation between both levels, and the voltage at which n peaks shifts slowly higher. However, note that in general the recombination rate depends on the occupancy of the defects. In addition, the DAP recombination is most effective close to midgap. Hence, for given $\Delta E = E_A - E_D$, the recombination current and the ideality factor are maximal for an almost symmetric distribution of E_A and E_D around midgap. Note that the behavior of the curves is symmetric to midgap for symmetric lifetimes $\tau^A_n = \tau^D_p$ and $\tau^D_n = \tau^A_p$. We choose $\sigma^A_n = \sigma^D_p$ and $\sigma^D_n = \sigma^A_p$, but the thermal velocities for electrons and holes are slightly different, so a slight asymmetry can be observed. Finally, for given ΔE and increasing distance of the energy pair from midgap, the DAP limitation, and therewith the saturation behavior, sets in at higher voltages. Hence also the voltage where n peaks is shifted to higher values.

We observed that, for equal CCS ($\sigma^A_n = \sigma^A_p$ and $\sigma^D_n = \sigma^D_p$), the saturation effect is negligible if the carrier densities are equal. Only in case of $\sigma_n \neq \sigma_p$ does the smaller capture coefficient provide a bottleneck for the recombination rate, which—for low voltages—can be bypassed by the coupled recombination.

Our simulations predict that a second peak in the ideality factor may appear at high voltages ($V_0 \sim 650$ mV). However, due to the saturation effect, the recombination rate in the damaged region becomes (above some bias V_0), dominated by recombination in other device regions. Accordingly, CDL recombination cannot influence n considerably above V_0. The values of V_0 and $n(V_0)$ depend on both N_t in the damaged region, the size of the damaged region in relation to the whole cell, and on the recombination rates outside the damaged region. In all solar cells we investigated, V_0 is considerably smaller than ≈650 mV, so this second peak in n does not appear in the dark I-V curve, which is the sum of recombination of all device parts.

If one of the coupled defects is very shallow, free carriers may tunnel into this defect. This effect is called trap-assisted tunneling (TAT).[14] For our set of parameters, this effect plays a negligible role in forward bias. However, in reverse bias, variations in the lattice relaxation energy $\varepsilon = S\hbar\omega$, where S is the Huang-Rhys factor and $\hbar\omega$ the effective phonon energy,[38] may strongly influence the breakdown-voltage.

C. Dependencies on the defect distribution

It is well known that heavily defected semiconductors have a broad distribution of defect levels within the bandgap. Therefore, we use a superposition of various DAPs to reproduce the measured data. Figure 8 shows the I-V and n curves of three PERL cells, where we made a 1 mm long scratch at the front surface with an indenter while exerting a load of 0.06 N, 0.09 N, or 0.26 N, respectively. We fitted these curve with simulations using only a combination of three different DAPs and obtain satisfactory fits. The heaviest load caused a 1 μm deep crater, so it is difficult to fit the experiment in the entire voltage range. Important is that the fit parameters reflect an increasing N with increasing indentation load, as summarized in Table I.

Using only three distinct DAPs is a simplification. In reality, there is a rather broad distribution of DAPs both w.r.t. N_t and the position in the bandgap. The effect of the width of a logarithmic Gaussian distribution of $N_t$on n is shown exemplarily in Fig. 9. A relatively narrow distribution has a small influence on the exact position of n. For broad distributions, the influence from defects, situated higher up

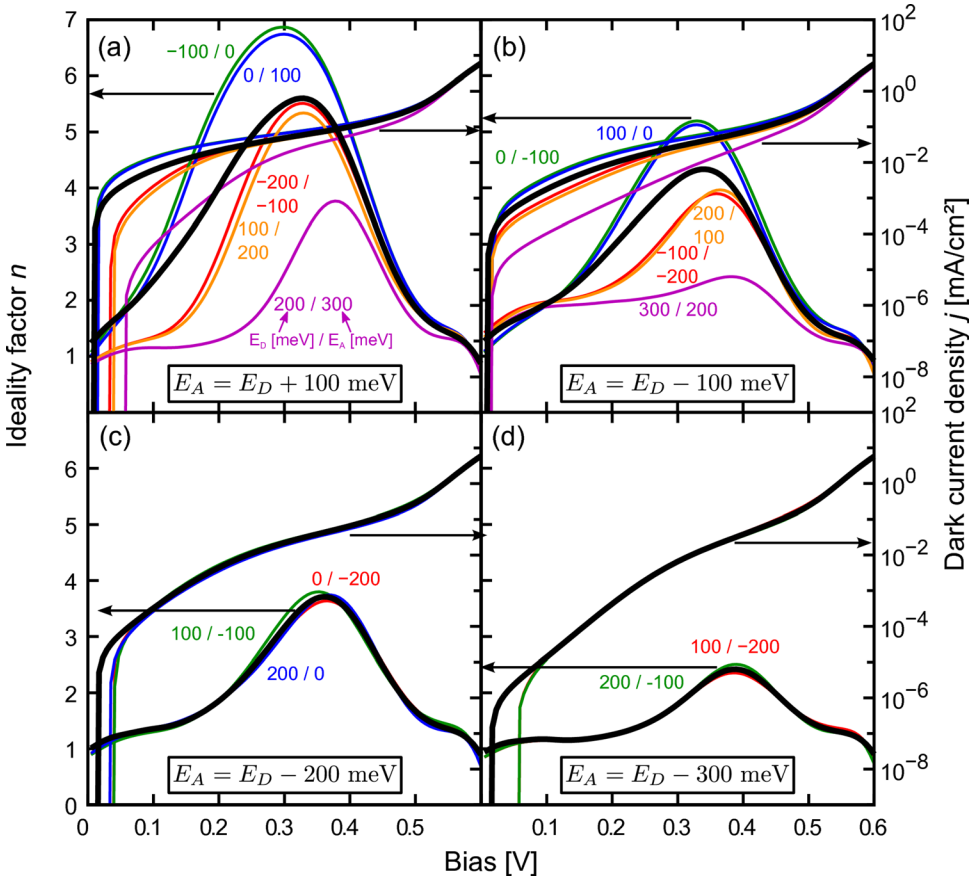

FIG. 7. (Color online) Dependence of the ideality factor on the energy levels E_D and E_A in respect to midgap for $N_t = 10^{21}$ cm^{-3}. The ideality factors are maximal for energy levels close to midgap and for small $|E_D - E_A|$.

than the peak-density $N_{t,0}$, becomes stronger, and the peak value of n shifts toward higher voltages.

Heavily defected regions are not expected to have only one specific type of defects, but to have a multitude of defect types extending over a broad range of energies. However, our study predicts that only deep DAPs lead to recombination currents that allow to reproduce the commonly observed shape of n as a function of bias. DAPs are characterized by $\sigma_n^D \gg \sigma_p^D$ and $\sigma_p^A \gg \sigma_p^D$, and hence, are most efficient for recombination compared to other coupled defects having $\sigma_n \approx \sigma_p$. Consequently, the DAPs dominate the overall recombination rate and, hence, the dark I-V curve. We like to stress here that different DAP-combinations may lead to the same satisfactory fit results. This is an important outcome, because our model yields the commonly observed shape of n whenever DAPs are present in an almost arbitrary, but broad distribution.

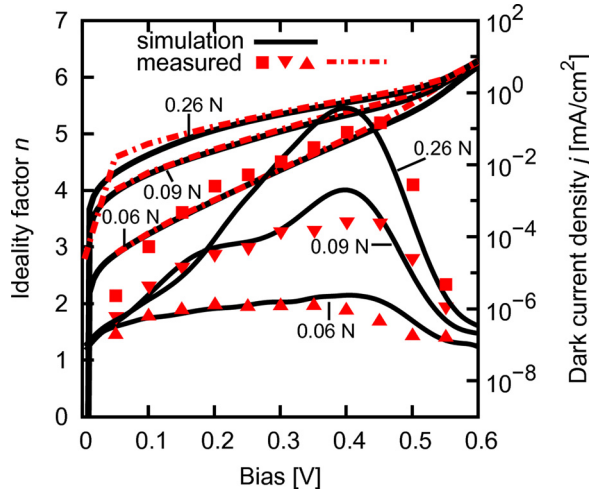

FIG. 8. (Color online) Measured I–V curves and the ideality factor n of PERL cells that received a 1 mm long scratch at the front surface with a load of 0.06 N, 0.09 N, or 0.26 N, respectively. The experiment is fitted with simulations (solid lines) using a combination of three different DAPs given in Table I.

D. Reverse characteristics

It is commonly observed[31,39] that the measured reverse characteristics [Fig. 1(c)] is influenced by the degree of disturbance. The higher the recombination current and the

TABLE I. Combinations of DAPs used to fit the I-V curve and the ideality factor n in Fig. 8.

force [N]	N_t [cm^{-3}]	E_D [meV]	E_A [meV]	fraction %
0.06	1×10^{21}	0	100	41.67
	1×10^{22}	0	−200	8.33
	1×10^{19}	100	0	50
0.09	1×10^{21}	0	100	26
	3×10^{21}	0	−200	42
	1×10^{21}	100	0	32
0.26	1×10^{21}	0	100	36
	3×10^{21}	0	100	29
	1×10^{22}	100	0	36

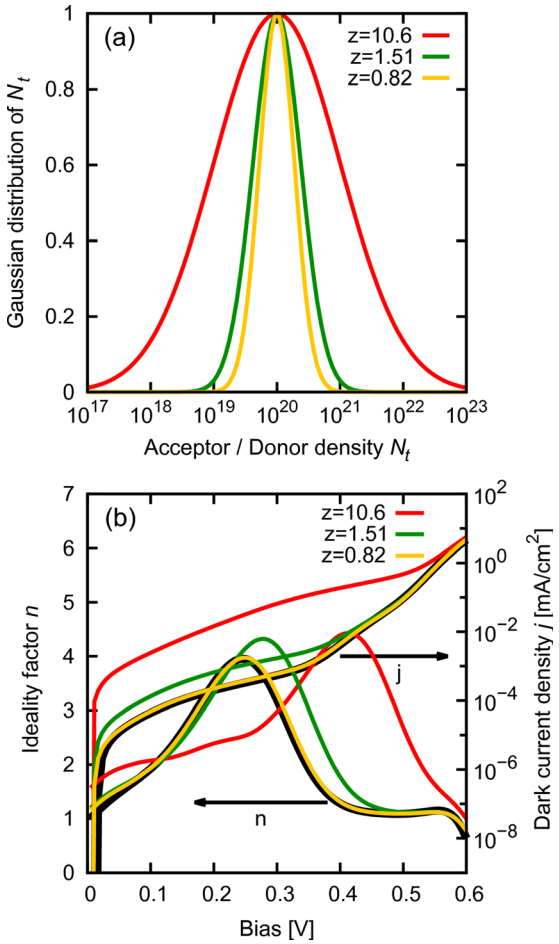

FIG. 9. (Color online) (a) Logarithmic Gaussian distributions $\propto \exp(-(\log(N_t - N_{t,0}))^2/z)$ at $N_{t,0} = 10^{20}$ cm^{-3} for different values of z. (b) Ideality factor (left axis) and dark current density (right axis) for the Gaussian distributions from (a). The black curve shows the results for a distinct peak density of $N_{t,0}$. The DAP energy levels are $E_D = 100$ meV and $E_A = 0$ meV.

ideality factor under forward bias, the stronger is the increase of the reverse I-V characteristics.

This effect is also observed in the simulation. Our simulations predict an almost ideal behavior of the reverse characteristics in the investigated voltage range ($I < 0.005$ mA/cm^2 at 6 V reverse bias) for defect densities $N_t < 10^{20}$ cm^{-3} (not shown here). For higher values of N_t, as e.g., $N_t = 10^{21}$ cm^{-3}, the correlation between high ideality factors n under forward bias and the increased current j under reverse bias is clearly visible, as displayed in Fig. 10. According to SRH-theory, j saturates in reverse direction according to the Shockley equation Eq. (1). In the presence of DAPs, each of the DAPs in the depletion region contributes to the total saturation current. Assuming a Schottky diode with an abrupt p-n junction, the extension of the depletion region z_{SCR} increases with $z_{SCR} \propto \sqrt{V_D - V}$ for an applied reverse bias $V < 0$, where V_D is the diffusion voltage.[40] Consequently, the number of DAPs contributing to the total current increases with increasing reverse bias. Thus, a square-root dependence of j on $V_D - V$ in the depletion region can be expected. Indeed, the simulated reverse currents in Fig. 10 are well described by a square-root dependence on V. Such a slightly sub-linear behavior is often observed for industrial cells,

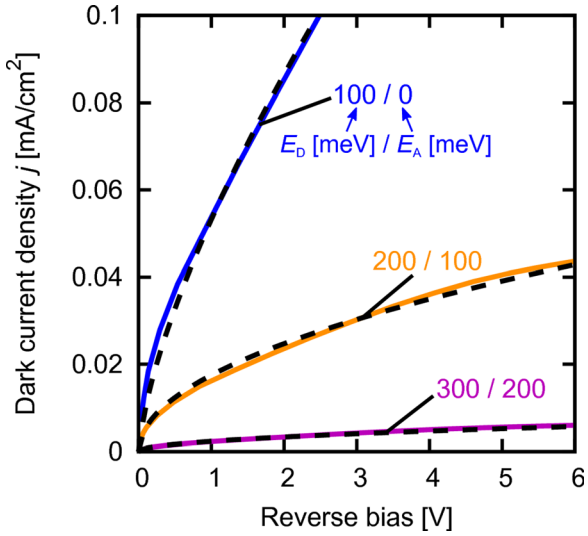

FIG. 10. (Color online) Simulated reverse characteristics with $N_t = 10^{21}$ cm^{-3} and for three different defect pairs.

showing $n > 2$ at forward bias. In contrast, the measured scratch-induced reverse currents in Fig. 1(c) do not show this behavior: they are Ohmic or slightly super-linear. It was found in Ref. 31 that the temperature dependence of these reverse currents can be explained by variable range hopping conduction according to Mott's theory[41] Since this type of conductivity requires charge transfer between many defects, it cannot be explained by our deep DAP model. For correctly describing the reverse characteristics our model had to be extended to include transitions between many levels.

E. Bias-dependent extension of the recombination region

So far, we have treated heavily defected regions that extend into a p-n junction depletion region. This is not the only common source of large shunt currents: they are often observed at the edge of solar cells as well, or possibly at micro-cracks within the cell. It was shown in Ref. 28 that n generally does not increase above 2 at a bias below 0.2 V if the p-n junction borders on the cell's edge that is passivated with a charged dielectric layer. Ref. 19 showed that a maximum possible surface saturation current-density of $j_{02,surf} = 2 \times 10^{-8}$ A/cm can be reached if the edge contains no or only a small density of fixed charges. This implies that the observed edge recombination currents with $j_{02,surf}$ as large as 10^{-5} A/cm and $n > 2$ cannot be interpreted by the simple recombination action of a plane crossing the p-n junction. Two major effects may cause such large edge recombination currents: firstly, a strongly reduced lifetime in the bulk close to the edge, or secondly, an inversion layer that extends the p-n junction depletion region at the front along the charged edge[19] or charged micro-crack down to the rear metal contact as shown in Fig. 5(b). The first case of a strongly reduced lifetime is treated in Ref. 42. We consider it as unlikely that this can be the source for the observed strong shunt currents, particularly if the edge region was etched. In the following, we investigate the case that the inversion layer extends from the front p-n junction to the rear contact. This

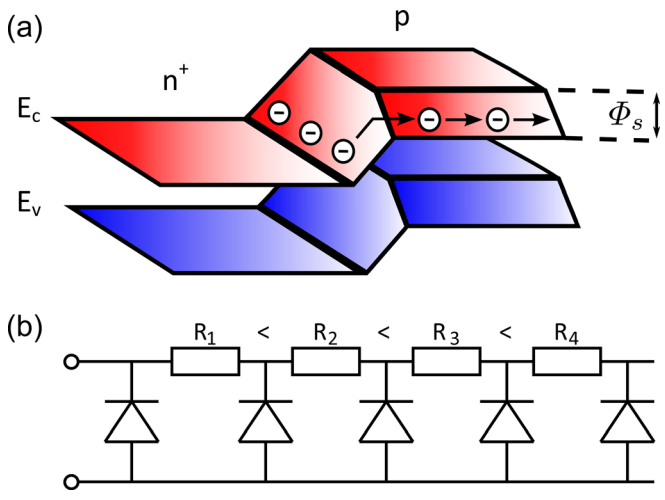

FIG. 11. (Color online) (a) Schematic representation of the 2-dimensional bandedge diagram of a forward biased p-n junction bordering to a positively charged surface at the front of the drawing. The barrier height across the p-n junction is lowered by the band bending at the surface, Φ_s, and hence forms a shunt-path to the rear contact. (b) Equivalent circuit of the device shown in (a).

may well happen in wafer material with $N_{dop} \approx 10^{16}$ cm^{-3}, as typically used for solar cells.

In Fig. 11, the chain of diodes represents the recombining p-type surface at different distances to the emitter. Using this circuit, the saturation behavior of the I–V characteristics can be easily understood. For low biases, where the recombination currents are low, the resistances of the diodes are high, and the series resistances R_i play only a minor role. Here, the recombination extends over the largest region. With increasing forward bias, the conductivity of the diodes increases. Thus, for the diodes situated further away from the emitter, the currents decrease, and thereby the region contributing to recombination becomes smaller, causing a saturation behavior. Note that this effect is different from the resistance-limited edge recombination effect considered in Refs. 16 and 17. There, only the emitter resistance was considered to limit the surface recombination current, which is independent of the bias. We employ Sentaurus-Device[35] to simulate the PERL cell of Fig. 5(b). We do not include DAP recombination, since we wish to model these two effects separately. The results are shown in Fig. 12. The voltage where n peaks depends on the values of Q_f and S_0.

In particular, the occurrence of saturation behavior in the dark I–V curves is limited by two critical values of the charge density, Q_1 and Q_2. Only for $Q_1 \leq Q_f \leq Q_2$, an ideality factor $n > 2$ may be obtained, whereas there is $n \leq 2$ for $Q_f < Q_1$ and $Q_f > Q_2$. The exact value of Q_1 and Q_2 depend on several cell parameters, as will be discussed below. For $Q_f < Q_1$, no inversion channel is formed, and thus, no saturation behavior is observed in the current densities j in Fig. 12(a), for charges below Q_1 given in Fig. 12(b). Consequently, the ideality factors n in Fig. 12(a) may reach but not exceed 2. This is in agreement with the observations made in Ref. 28. Generally, $n > 2$ can only be realized if Q_f is sufficiently high so the surface is close to inversion already at thermal equilibrium. This is observed for charges $Q > Q_1$, where the resistance limitation of the current through the inversion layer causes very high ideality factors. The influence of this limitation increases with increasing S_0 and hence, the maximum of n increases with S_0. In comparison with the DAP recombination, the peaks of n are typically more narrow and may reach very high values ($n \approx 30$). For further increasing charge densities $Q > Q_2$, the series resistance R_s becomes negligible, the saturation behavior of the current density j vanishes and, thus, $n \leq 2$. The critical charge densities Q_1 and Q_2 depend on both S_0 and N_A, as shown in Fig. 12(b). The increase of R_s with S_0 causes Q_1 and Q_2 to increase. Further, the charge density that causes inversion in thermal equilibrium reduces with decreasing base doping, and hence Q_1 and Q_2 decrease. As R_s increases with increasing distance to the emitter, thicker cells require higher charges (or voltages) to achieve a continuous inversion channel from the emitter to the rear contact. Hence, Q_1 and Q_2 increase (not plotted here). It is generally observed that cells with a high n under forward bias tend to have reverse characteristics that are Ohmic or slightly super-linear. Figure 12(c) shows that this effect cannot be explained with this surface model, since the band bending is reduced or

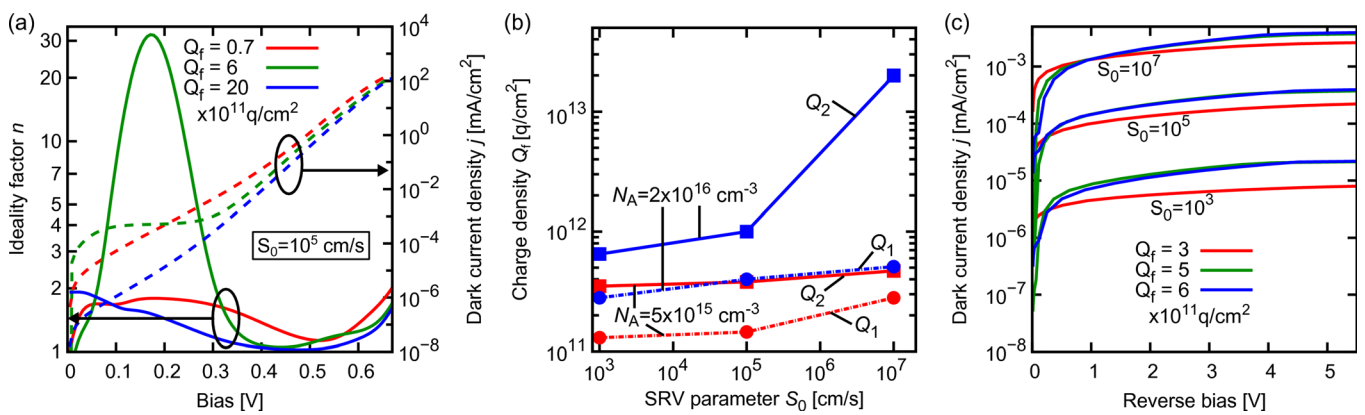

FIG. 12. (Color online) (a) Simulated I–V curves and ideality factors of a PERL cell with $N_A = 2 \times 10^{16}$ cm^{-3} and an inversion layer along its edge as shown in Fig. 5. The charge Q_f is varied for $S_0 = 10^5$ cm/s. (b) Critical charge densities Q_1 (dashed lines) and Q_2 (continuous lines) for two base dopant densities $N_A = 2 \times 10^{16}$ cm^{-3} (blue lines) and $N_A = 5 \times 10^{15}$ cm^{-3} (red lines) in dependence on S_0. (c) Reverse characteristics of cells with $N_A = 2 \times 10^{16}$ cm^{-3} for different values of S_0 and Q_f which yield.

inverted under reverse bias, such that the depletion or inversion layer vanishes. This surface model can only explain shunt currents in forward bias. However, as the current densities are low, it does also not hamper the occurrence of the non-saturating effects as obtained from the DAP model. Hence, it is definitely possible that both DAPs and charged edges or micro-cracks, if present simultaneously, may contribute to high ideality factors under forward bias.

IV. CONCLUSIONS

We have presented direct experimental evidence that the ideality factor n of the I–V characteristics of crystalline Si solar cells increases beyond 2 for an increasing amount of disturbance by cleaving, laser cutting or scratching. These experimental findings are reproduced by device modeling using donor-acceptor-pair (DAP) recombination via deep levels. We are able to reproduce both measured ideality factors and the dark current densities. These simulations explain the experimentally observed increase of n with increasing defect density. We do not need a particular set of defects to reproduce the commonly observed shape of n as a function of bias. It is only important that DAPs are present in the defect distribution. They are most efficient for recombination compared to other coupled defects and hence dominate the overall recombination rate. Our model yields the commonly observed shape of n whenever there are DAPs present in an almost arbitrary broad distribution. Additionally, our model yields slightly sub-linear reverse-characteristics, as frequently observed for industrial-type cells with $n > 2$ for forward bias. This was explained by an increasing number of DAPs contributing with increasing reverse bias to the current. We also investigated an other source of shunt currents: an inversion layer extending from the front p-n junction to the rear contact via the cell's edge or along micro-cracks. Generally, $n > 2$ can only be realized if Q_f is sufficiently high so the surface is close to inversion already at thermal equilibrium. In comparison with the DAP recombination, the peaks of n are typically more narrow and may reach very high values. However, this surface model can only explain shunt currents in forward bias. Our simulations explain, possibly for the first time, the observation made with lock-in thermography that the ideality factor increases with increasing disturbance, in both forward and revers bias.

ACKNOWLEDGMENTS

We acknowledge the experimental cooperation with H. Leipner (Halle University) in performing the variable load scratching. We thank J. Zhao and M. Green (both UNSW) for providing us the opportunity to perform the cleavage and laser-scribing experiments at their institute.

[1]W. Shockley and W. T. Read, Phys. Rev. **87**, 835 (1952).
[2]R. N. Hall, Phys. Rev. **87**, 387 (1952).
[3]W. Shockley, Bell Sys. Tech. J. **28**, 435 (1949).
[4]C.-T. Sah, R. N. Noyce, and W. Shockley, Proc. IRE **45**, 1228 (1957).
[5]S. C. Choo, Solid State Electron. **11**, 1069 (1986).
[6]A. Nussbaum, Phys. Status Solidi A **19**, 441 (1973).
[7]P. J. Anderson and M. J. Buckingham, Electron. Lett. **13**, 496 (1977).
[8]K. Lee and A. Nussbaum, Solid State Electron. **23**, 655 (1980).
[9]R. Corkish and M. A. Green, J. Appl. Phys. **80**, 3083 (1996).
[10]J. Pallarès, L. F. Marsal, X. Correig, J. Calderer, and R. Alcubilla, Solid State Electron. **41**, 17 (1997).
[11]K. R. McIntosh, P. P. Altermatt, and G. Heiser, in *Proc. 16th EU PVSEC* (James and James, Glasgow, UK, 2000), pp. 243–246.
[12]H. J. Queisser, Solid State Electron. **1**, 1 (1962).
[13]A. Kaminski, J. J. Marchand, H. E. Omari, A. Laugier, Q. N. Le, and D. Sarti, in *Proc. 25th IEEE PVSC* (Washington, D. C., 1996) pp. 573–576.
[14]A. Schenk and U. Krumbein, J. Appl. Phys. **78**, 3185 (1995).
[15]J. Beier and B. Voss, in *Proc. 23th IEEE PVSC* (Louisville, KY, 1993), pp. 321–324.
[16]K. R. McIntosh, "Lumps, humps and bumps: Three detrimental effects in the current-voltage curve of silicon solar cells," Ph.D. thesis, (UNSW, School of Electrical Engineering, Sydney, 2001).
[17]K. R. McIntosh and C. B. Honsberg, in *Proc. 16th EU PVSEC* (James and James, London, UK, 2000), pp. 1651–1654.
[18]A. S. H. van der Heide, A. Schönecker, J. H. Bultman, and W. C. Sinke, Prog. Photovolt. Res. Appl. **13**, 3 (2005).
[19]R. Kühn, P. Fath, and E. Bucher, in *Proc. 28th IEEE PVSC* (Anchorage, AL, 2000) pp. 116–119.
[20]O. Breitenstein, M. Langenkamp, O. Lang, and A. Schirrmacher, Sol. Energy Mater. Sol. Cells **65**, 55 (2001).
[21]O. Breitenstein, M. Langenkamp, J. P. Rakoniaina, and J. Zettner, in *Proc. 17th EU PVSEC* (Munich, Germany, 2001), pp. 1499–1502.
[22]A. Hauser, G. Hahn, M. Spiegel, H. Feist, O. Breitenstein, and P. Rakotoniaina, in *Proc. 17th EU PVSEC* (Munich, Germany, 2001), p. 1739.
[23]O. Breitenstein and M. Langenkamp, *Lock-in Thermography - Basics and Use for Functional Diagnostics of Electronic Components* (Springer, Berlin, 2003).
[24]J. J. Hopfield, D. G. Thomas, and M. Gershenzon, Phys. Rev. Lett. **10**, 162 (1963).
[25]D. G. Thomas, J. J. Hopfield, and W. M. Augistyniak, Phys. Rev. **140**, A202 (1965).
[26]S. J. Robinson, S. R. Wenham, P. P. Altermatt, A. G. Aberle, G. Heiser, and M. A. Green, J. Appl. Phys. **78**, 4740 (1995).
[27]M. Y. Ghannam and R. P. Mertens, IEEE Electron. Device L. **10**, 4740 (1989).
[28]P. P. Altermatt, A. G. Aberle, J. Zhao, A. Wang, and G. Heiser, Sol. Energy Mater. Sol. Cells **74**, 165 (2002).
[29]E. H. Rhoderick and R. H. Williams, *Metal-Semiconductor Contacts* (Clarendon, Oxford, UK, 1988), pp. 39 and 99.
[30]A. G. Aberle, P. P. Altermatt, G. Heiser, S. J. Robinson, A. Wang, J. Zhao, U. Krumbein, and M. A. Green, J. Appl. Phys. **77**, 3491 (1995).
[31]O. Breitenstein, P. P. Altermatt, K. Ramspeck, and A. Schenk, in *Proc. 21st EU PVSEC* (Dresden, Germany, 2006), pp. 625–628.
[32]D. Macdonald and L. J. Geerligs, Appl. Phys. Lett. **85**, 4061 (2004).
[33]M. Lax, J. Phys. Chem. Solids **8**, 66 (1959).
[34]S. Gasiorowicz, *Quantum Physics* (John Wiley and Sons, New York, 1974), p. 319.
[35]Sentaurus-Device, available at www.synopsys.com/products/tcad/tcad.html Synopsys Inc., Mountain View, CA.
[36]P. P. Altermatt, G. Heiser, A. G. Aberle, A. Wang, J. Zhao, S. J. Robinson, S. Bowden, and M. A. Green, Prog. Photovoltaics **4**, 399 (1996).
[37]P. P. Altermatt, A. Schenk, and F. Geelhaar, J. Appl. Phys. **93**, 1598 (2003).
[38]A. Schenk, Solid State Electron. **35**, 1558 (1992).
[39]O. Breitenstein, J. Bauer, A. Lotnyk, and J.-M. Wagner, Superlattices Microstruct. **45**, 182 (2009).
[40]H. Ibach and H. Lüth, *Festkörperphysik,* 6th ed. (Springer, Berlin, 2002), p. 411.
[41]N. Mott, *Metal-Insulator Transitions* (Taylor and Francis, London, 1990).
[42]S. Steingrube, P. P. Altermatt, D. S. Steingrube, J. Schmidt, and R. Brendel, J. Appl. Phys. **108**, 014506 (2010).